Global warming accelerates uptake of atmospheric mercury in regions experiencing glacier retreat

Xun Wang[a], Ji Luo[b], Wei Yuan[a,c], Che-Jen Lin[d,e], Feiyue Wang[f], Chen Liu[a,c], Genxu Wang[b], and Xinbin Feng[a,c,g,1]

[a]State Key Laboratory of Environmental Geochemistry, Institute of Geochemistry, Chinese Academy of Sciences, Guiyang 550081, China; [b]Key Laboratory of Mountain Surface Processes and Ecological Regulation, Institute of Mountain Hazards and Environment, Chinese Academy of Sciences, Chengdu 610041, China; [c]University of Chinese Academy of Sciences, Beijing 100049, China; [d]Center for Advances in Water and Air Quality, Lamar University, Beaumont, TX 77710; [e]Department of Civil and Environmental Engineering, Lamar University, Beaumont, TX 77710; [f]Centre for Earth Observation Science, and Department of Environment and Geography, University of Manitoba, Winnipeg, MB R3T 2N2, Canada; and [g]Center for Excellence in Quaternary Science and Global Change, Chinese Academy of Sciences, Xian 710061, China

Edited by Zhi-Sheng An, Institute of Earth Environment, Xi'an, China, and approved December 6, 2019 (received for review April 22, 2019)

As global climate continues to warm, melting of glaciers releases a large quantity of mercury (Hg) originally locked in ice into the atmosphere and downstream ecosystems. Here, we show an opposite process that captures atmospheric Hg through glacier-to-vegetation succession. Our study using stable isotope techniques at 3 succession sites on the Tibetan Plateau reveals that evolving vegetation serves as an active "pump" to take up gaseous elemental mercury (Hg^0) from the atmosphere. The accelerated uptake enriches the Hg pool size in glacier-retreated areas by a factor of ∼10 compared with the original pool size in the glacier. Through an assessment of Hg source–sink relationship observed in documented glacier-retreated areas in the world (7 sites of tundra/steppe succession and 5 sites of forest succession), we estimate that 400 to 600 Mg of Hg has been accumulated in glacier-retreated areas (5‰ of the global land surface) since the Little Ice Age (∼1850). By 2100, an additional ∼300 Mg of Hg will be sequestered from the atmosphere in glacier-retreated regions globally, which is ∼3 times the total Hg mass loss by meltwater efflux (∼95 Mg) in alpine and subpolar glacier regions. The recapturing of atmospheric Hg by vegetation in glacier-retreated areas is not accounted for in current global Hg models. Similar processes are likely to occur in other regions that experience increased vegetation due to climate or land use changes, which need to be considered in the assessment of global Hg cycling.

global warming | glacier retreat | atmospheric mercury deposition

To alleviate global mercury (Hg) pollution, international efforts to curb anthropogenic Hg emissions have culminated in the Minamata Convention on Mercury, a legally binding international treaty that went into force in 2017. The execution of this convention and assessment of regulatory efforts rely on a clear understanding of global Hg sources, sinks, and their dynamics. Major uncertainties exist in our understanding on Hg transport and accumulation in remote ecosystems due to the complex interplays of biological, orographic, and climatic factors (1–4). The cycling of Hg in subpolar and alpine regions is increasingly modulated by global climate changes (3, 5). Specifically, the alpine and subpolar glaciers (6, 7) have been shrinking rapidly due to accelerated warming in recent decades (8, 9). Earlier studies show that Hg efflux from glaciers to meltwater-fed ecosystems causes a distinct risk of bioaccumulation of Hg, especially methyl Hg, in ecosystems (10–13). As glaciers retreat, vegetation tends to establish in the retreated areas, and an entirely new ecosystem (e.g., forest, steppe, and tundra) evolves over time. Vegetation uptake of elemental Hg (Hg^0) from the atmosphere has long been recognized as an important pathway of atmospheric Hg deposition (3, 14, 15). However, little is known on the significance of Hg uptake by vegetation established in glacier-retreated area.

The Himalaya–Tibetan Plateau (TP) region is home to the largest and highest mountain ranges where ∼15% of the world's glacier mass resides (8). This study determines the source–sink relationship and accumulation pathways of Hg during the glacier-to-vegetation succession by investigating the signatures of stable Hg isotopes at a whole-ecosystem scale in 3 forest chronosequences of the glacier-retreated areas in the TP. The chronosequences span 1 to 2 km within a narrow altitude range at the Hailuogou Glacier, Mingyong Glacier, and Midui Glacier (the site description is detailed in *SI Appendix*). The glacier retreat period ranged from 1830 to 2015 at Hailuogou and from 1925 to 2015 at Mingyong and Midui (*SI Appendix*, Figs. S1–S3). We quantified Hg pool sizes in the soil horizons across the sites. The Hg isotopic compositions of the air, precipitation, vegetation, rock, and soil samples (*SI Appendix*, Tables S1–S14) are measured to infer the Hg sources and their relative contributions during vegetation succession. We further assessed Hg source–sink transitions in documented glacier-retreated areas in the world, including 7 sites of tundra/steppe succession and 5 sites of forest succession, and their implications for the global Hg cycling.

Mercury Sources Determined by Stable Isotope Composition

The soil profiles show the organic soil and C horizon soil (soil parent horizon) overlying the bedrock. The absence of a distinct A (mineral) horizon is attributed to the relatively short time period of vegetation succession. Due to the difference in plant productivity, the thickness of the organic soil horizon in the glacier-retreated area ranges from 0 to 10 cm at Hailouguo after 125 y of succession to as thin as 0 to 5 cm at Mingyong and Midui after 90 y of recession. At all sites, the soil is not well developed beyond 20-cm C soil. Therefore, the soil profile at Hailuogou is classified into 5 layers of organic soil, 0- to 5-, 5- to 10-, 10- to 15-, and 15- to 20-cm C soil, whereas at Mingyong and Midui, soil profile is divided into 0- to 5-, 5- to 10-, 10- to 15-, and 15- to 20-cm soil horizons.

Significance

In this study, we identify a process that recaptures atmospheric Hg in glacier-retreated areas driven by global warming. Melting of glaciers is known to release Hg originally locked in ice into the atmosphere and downstream ecosystems. Recession of glaciers promotes rapid establishment of vegetative ecosystems that capture more atmospheric Hg over the long run than the Hg released from glacier melting. The increased vegetative biomass driven by climate change can result in significant changes in global Hg cycling.

Author contributions: X.W. and X.F. designed research; X.W., J.L., W.Y., C.L., G.W., and X.F. performed research; X.W. and X.F. contributed new reagents/analytic tools; X.W., W.Y., C.-J.L., F.W., and X.F. analyzed data; and X.W., C.-J.L., and F.W. wrote the paper.

The authors declare no competing interest.

This article is a PNAS Direct Submission.

[1]To whom correspondence may be addressed. Email: fengxinbin@vip.skleg.cn.

This article contains supporting information online at https://www.pnas.org/lookup/suppl/doi:10.1073/pnas.1906930117/-/DCSupplemental.

In general, the soil Hg concentrations gradually decrease with depth at Hailuogou (*SI Appendix*, Fig. S4), often 1 order of magnitude higher in the surface organic soil than in the deep C-horizon soil and bedrock. The soil Hg concentrations in Oe (underlain by a partially decomposed layer) and Oa (a very dark layer of well-decomposed humus) are higher than those in Oi (litter and twigs) at Hailuogou, which can be attributed to the greater litter mass loss during the initial litter decomposition, leading to Hg accumulation in Oe and Oa. This is consistent with earlier studies showing Hg concentration changes during litter decomposition (16, 17) and also supported by the increase in the Hg/C ratio from Oi to Oa (*SI Appendix*, Fig. S5). The Hg concentrations in the 0- to 5-cm soil at Mingyong and Mitui are 1 to 3 times higher than the values in 15- to 20-cm soil and bedrock (*SI Appendix*, Fig. S6). Below the 5-cm C soil (Hailuogou) or 15- to 20-cm soil (Mingyong and Midui), the soil Hg concentrations are comparable with the values in the bedrock ($P = 0.902$ and 0.923, respectively; ANOVA). These suggest that the influence of vegetation succession in the glacier-retreated areas on Hg biogeochemical processes is limited to the surface soil over a temporal scale of ∼100 y. Therefore, we focus only on the organic soil and 0- to 5-cm C soil at Hailuogou and 0- to 15-cm soil at Mingyong and Midui.

The sources of Hg in the surface soil may originate from atmospheric deposition of Hg^0 (e.g., atmospheric Hg^0 uptake by vegetation with subsequent deposition to soil following plant detritus), from atmospheric Hg(II) (e.g., via precipitation), and from weathering of geological Hg in bedrocks. Recent advancement of stable Hg isotope techniques makes it possible to delineate the origins and accumulation pathways. Mercury isotopes undergo both mass-dependent fractionation (reported as δ^{202}Hg) and mass-independent fractionation (MIF; reported as Δ^{199}Hg, Δ^{200}Hg, and Δ^{201}Hg) in the environment (18). The MIF signatures of Hg isotopes have been shown to be a useful tracer to identify specific sources (4, 18, 19). Three distinct MIF endmembers were identified (Fig. 1), including the mean MIF observed in the canopy foliage, lichen, and moss samples as the signature of atmospheric Hg^0 input; the MIF in the precipitation samples as the signature of atmospheric Hg(II) input; and the MIF in the bedrock and deep soil samples of the C horizon as the signature of geological Hg.

Fig. 1 and *SI Appendix*, Tables S7–S14 show that Δ^{199}Hg and δ^{202}Hg signatures in the soil samples of Hailuogou, Mingyong, and Midui generally increase with the depth, while Δ^{200}Hg values are close to 0 rather than typically positive values found in atmospheric water. The δ^{202}Hg values of surface soil at Hailuogou are much closer to the values of vegetation due to the higher plant productivity at this site, whereas the values at Mingyong and Midui are closer to those found in deep soil (*SI Appendix*, Figs. S7–S15).

The large differences in δ^{202}Hg at these sites allow for developing a constrained Hg MIF mixing model with good confidence (Eqs. **1**–**4**; details are in *Methods* and *SI Appendix*). The triple-endmember mixing model using δ^{202}Hg as the constrain shows that the Hg source fractions in the soil depend on the lapsed time after glacier retreat. At Hailuogou where glacier-to-vegetation succession has undergone 125 y with a high plant productivity, atmospheric Hg^0 is the dominant source for the organic soil (Fig. 2 and *SI Appendix*, Fig. S16), accounting for 36 to 96% (mean = 71%, median = 69%) of the total Hg. *SI Appendix*, Fig. S16 shows that the Oi has the highest atmospheric Hg^0 fraction (>85%) followed by Oe (66 to 84%), Oa (36 to 93%, mean = 66%, median = 68%), and 0- to 5-cm C soil (35 to 40%). This agrees with earlier findings that atmospheric Hg^0 deposition is the dominant Hg source on the forest floor (4, 15, 20–22) and in organic soil of the biome of tundra/steppe (3, 20). In contrast, at the sites with smaller accumulated plant biomass in Mingyong and Midui where the succession has only taken place in the past 90 y, atmospheric Hg^0 deposition accounts for only 20 to 77% (mean = 50%, median = 60%) and 9 to 34% (mean = 24%, median = 30%), respectively, of the Hg in the 0- to 5-cm soil (*SI Appendix*, Fig. S17). Atmospheric Hg(II) has the smallest contribution, accounting for 2 to 18% of total Hg in organic soil at Hailuogou and 3 to 11% and 3 to 7% in the 0- to 5-cm soil at Mingyong and Midui, respectively (*SI Appendix*, Figs. S16 and S17). As expected, the contribution of geological sources to soil Hg increases with depth at all 3 sites, reaching up to 70 to 95% at the deepest depth above the bedrock at Mingyong and Midui (*SI Appendix*, Fig. S17).

Overall, we found that soil Hg originated primarily from atmospheric sources at Hailuogou and from geological sources at Midui. This is also supported by a significant positive correlation ($r = 0.8235$, $P < 0.001$, $n = 93$) between the content of soil organic carbon (SOC), which can serve as a surrogate for plant productivity in glacier-retreated regions (4, 17), and the fraction of atmospheric Hg^0 in soil. Higher plant productivity at Hailuogou thus induces greater atmospheric Hg^0 accumulation than at Mingyong and Midui.

Rapid Hg Accumulation during Vegetation Development

Over the 125-y period, the total Hg pool size (6,434 ± 1,911 g km^{-2}, mean ± 1 SD) at Hailuogou is comparable with those found in organic soil of mature coniferous forest ecosystems in North America and Europe (3,400 to 6,800 g km^{-2}) (23–26). The Hg MIF mixing model shows that the Hg pool derived from atmospheric deposition increases continuously in the organic layer and C-horizon soil (0 to 5 cm) at Hailuogou (Fig. 2). Over the 125-y period, the soil accumulates a total of 4,802 ± 3,122 g Hg km^{-2} from atmospheric Hg^0 deposition and 509 ± 1,589 g Hg km^{-2} from atmospheric Hg(II) deposition. The total atmospheric pool size [derived from the sum of atmospheric Hg^0 and Hg(II) sources] in the organic layer is ∼17 times larger than in the 0- to 5-cm C soil at Hailuogou, suggesting that the organic soil is the most important reservoir storing atmospheric Hg deposition in forest ecosystems. Over a 90-y period of vegetation succession (Fig. 2), the Hg pool sizes contributed by atmospheric Hg^0 and Hg(II) at Mingyong are 1,580 ± 978 and 275 ± 689 g km^{-2}, respectively. At Midui, these amount to 908 ± 708 g km^{-2} for atmospheric Hg^0 and 201 ± 613 g km^{-2} for atmospheric Hg(II) over the same 90-y period. Overall, we estimate that 90 ± 71% of the total Hg pool size derives from atmospheric Hg^0 deposition at Hailuogou over a 125-y period and 85 ± 63% at Mingyong and 80 ± 64% at Midui over a 90-y period. The accumulation rate of atmospheric Hg^0 at Hailuogou is 38.4 ± 24.9 μg m^{-2} y^{-1} over the past 125 y, and they are 17.5 ± 10.9 μg m^{-2} y^{-1} at Mingyong and 10.1 ± 7.9 μg m^{-2} y^{-1} at Midui over the 90-y period.

Variation of the Hg pool contributed by atmospheric deposition in glacial-retreated regions elsewhere is estimated using an SOC–Hg model (Fig. 3; details are in *SI Appendix*). This includes 7 sites of tundra/steppe succession and 5 sites of forest succession (Fig. 3). Applying the 80 ± 64% (lowest fraction in this study) contribution of atmospheric Hg^0 to the total Hg pool size in soil, the accumulation rate of atmospheric Hg^0 is 9.5 ± 7.1 μg m^{-2} y^{-1} ($n = 7$) in the global tundra–shrub/steppe succession and 14.7 ± 10.6 μg m^{-2} y^{-1} ($n = 8$) in the global forest succession (*SI Appendix*, Table S16). Amos et al. (27) suggested an average of 12.3 ± 9.0 μg m^{-2} y^{-1} total Hg accumulation rate in peat during the preindustrial period and a present-day accumulation rate of 21.1 ± 9.1 μg m^{-2} y^{-1} ($n = 21$). Given that 80 to 90% of peat Hg is attributed to atmospheric Hg^0 deposition (3, 20), we estimate that the accumulation rate of atmospheric Hg^0 in the tundra–shrub/steppe succession is comparable with the average rate in peat during preindustrial period but significantly lower than the present-day accumulation rate (27). This suggests that forest chronosequences potentially provide a new record that can be used for deducing the enhanced ratio of Hg at present day compared with that in the preindustrial era. Litterfall Hg deposition has been suggested as the main contributor for atmospheric Hg^0 deposition in forest ecosystems (5, 28). The

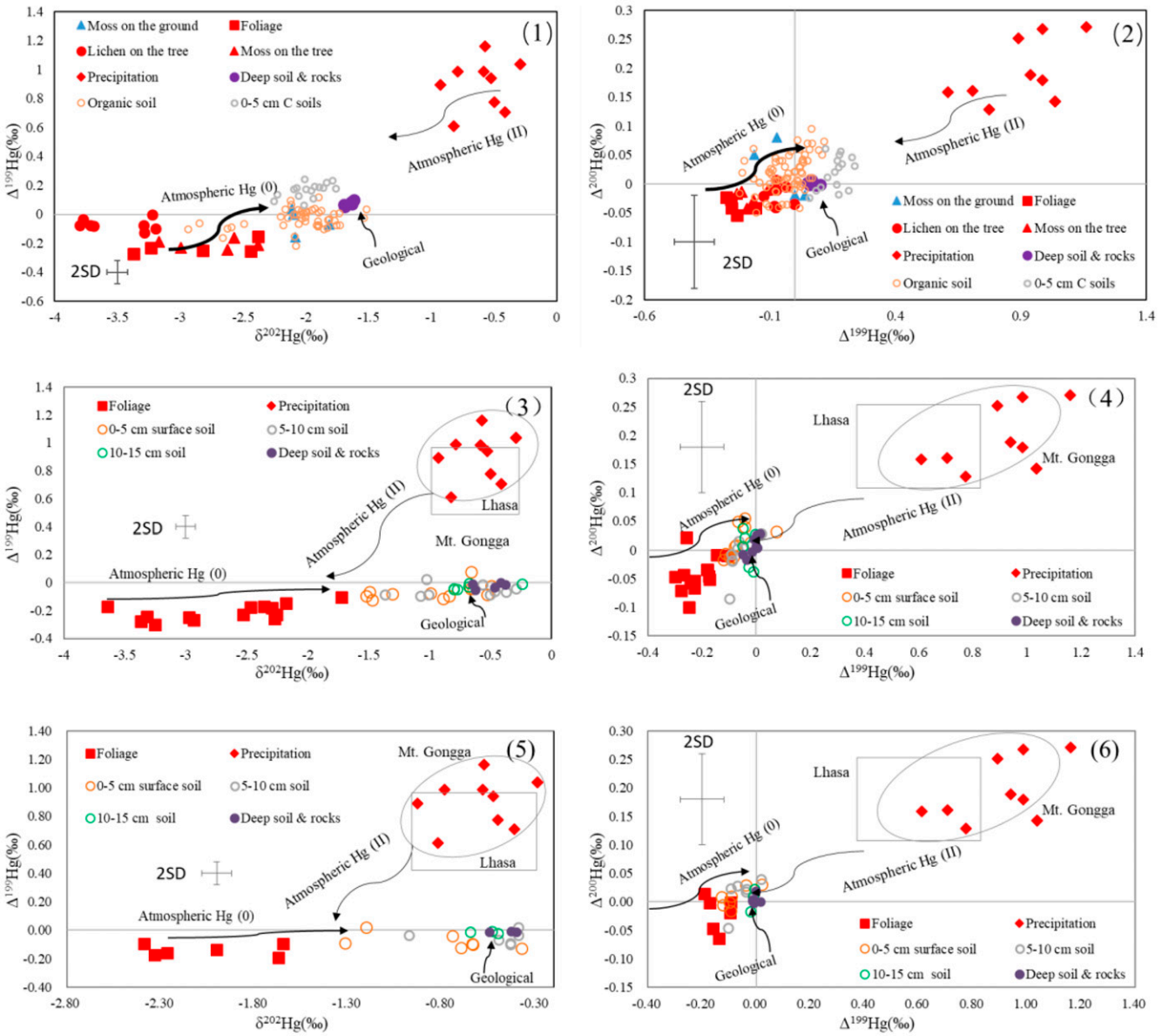

Fig. 1. Mercury isotopic signatures in the forest chronosequence zone: (*1* and *2*) at Hailuogou, (*3* and *4*) at Mingyong, and (*5* and *6*) at Midui. 2SD, 2 standard deviations.

estimated accumulation rates of atmospheric Hg^0 during the global forest successions are comparable with the average value of litterfall Hg deposition (15.2 ± 8.4 μg m^{-2} y^{-1}) in global temperate/boreal forest ecosystems (28).

Over a relatively short timescale, climate warming leads to an Hg release from retreated glaciers (12, 13, 29). However, glacier retreat facilitates atmospheric Hg fixation in newly developed vegetation and soil over the long term. The original Hg pool size in the glacier at Hailuogou is 355 ± 71 g km^{-2} as determined by the Hg concentration (3.0 ± 0.6 ng L^{-1}) in the glacier ice cores and the mean depth (~130 m in the Little Ice Age) of the glacier (*SI Appendix*, Table S15). The total Hg pool size in organic soil reaches this level in 30 y after glacier retreat (Fig. 2) and increases to 12 times greater after 125 y. The Hg pool sizes over the 90-y vegetation succession at Mingyong and Midui (Fig. 2) are also 1 order of magnitude higher than the original glacier Hg pool sizes based on the estimated Hg concentration in ice cores (*SI Appendix*, Table S15) and ice glacier volumes in the Little Ice Age. Fig. 3 shows that the Hg pool size increases by a factor of 2 to 5 in global tundra and steppe glacier-retreated regions and by a factor of 4 to 10 in forested regions within 80 to 125 y of vegetation succession. These imply that, within a few decades after glacier retreat, vegetation succession can fully compensate the Hg loss due to glacier melting and serve as an increasingly large atmospheric Hg sink.

Implications

The global mean air temperature is projected to increase by 2.0 to 4.9 °C (median: 3.2 °C) by 2100 (30). This will potentially cause melting of 21 to 27% of alpine and subpolar glaciers globally (31). Regions such as western Canada and the European Alps may lose as much as 70 to 75% of their alpine glaciers (31–34). Although Hg mass in forest succession reaches a plateau after 120 to 200 y after glacier retreat (Figs. 2 and 3), atmospheric Hg^0 uptake in glacier-retreated regions is anticipated to accelerate because of the formation of new vegetation ecosystems and

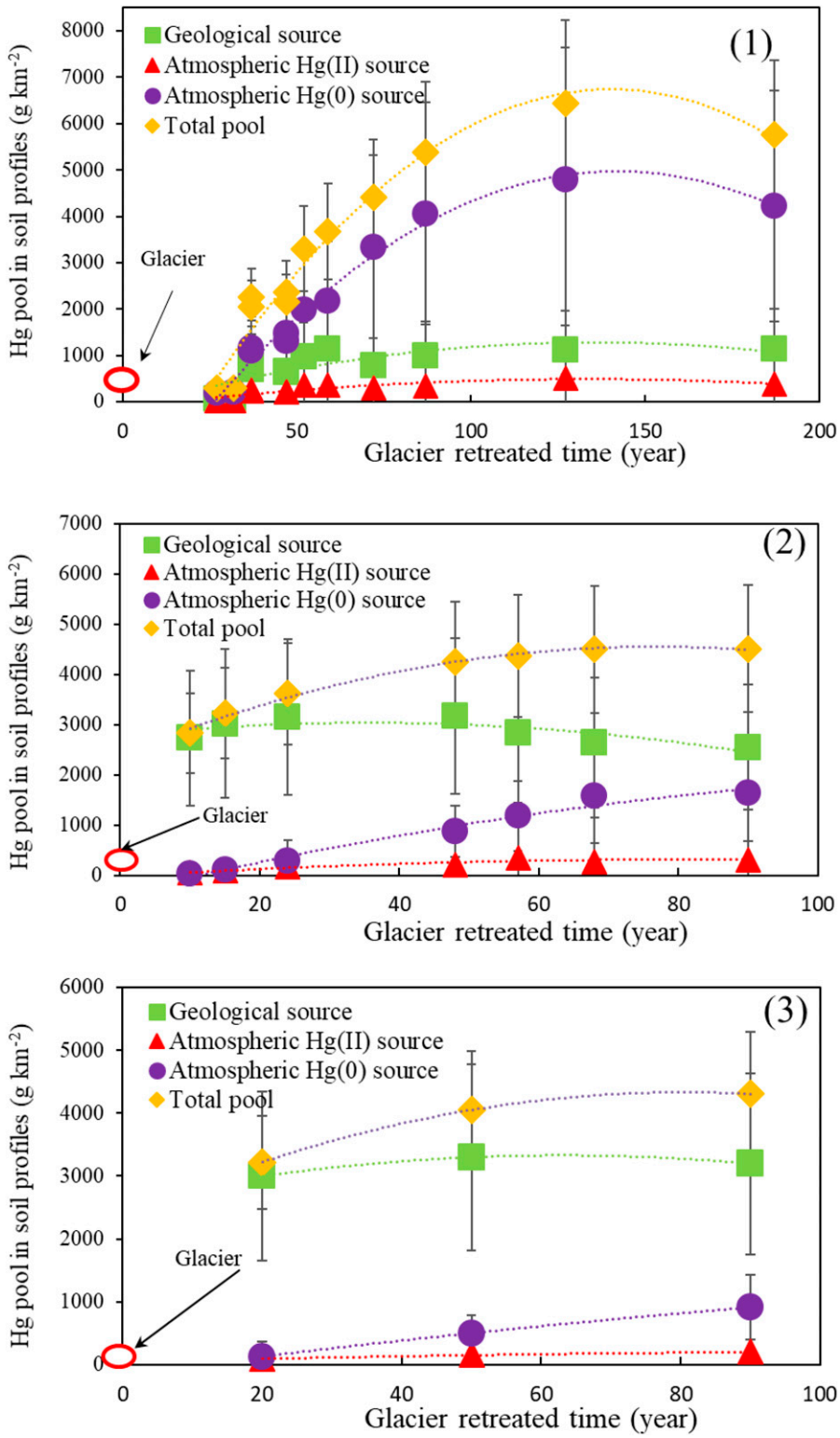

Fig. 2. Mercury source fractions (mean ± 1 SD) in the forest chronosequence zone: (*1*) organic soil and 0- to 5-C soil profiles at Hailuogou, (*2*) 0- to 15-cm soil profiles at Mingyong, and (*3*) 0- to 15-cm soil profiles at Midui. The source fractions are the summary of specific fraction in each soil profile in *SI Appendix*, Figs. S16 and S17. The uncertainties are discussed in detail in *SI Appendix*.

the continuous accumulation facilitated by vegetative biomass. The current rate of Hg mass loss in subpolar and alpine glacier regions is estimated to be 0.4 to 0.6 Mg y^{-1}, assuming a water loss rate of 200 to 300 Gt y^{-1} (31) and an mean Hg concentration of 2 pg g^{-1} (*SI Appendix*, Table S15). By 2100, the total Hg mass loss from glacier melt is projected to be ∼95 Mg (∼47,000 Gt water loss because of higher glacier retreat rates in the future [31]), while the Hg mass captured by the new ecosystems in glacier-retreated areas is ∼2 times greater (∼300 Mg based on the present-day mean Hg^0 accumulation rate and predicted new

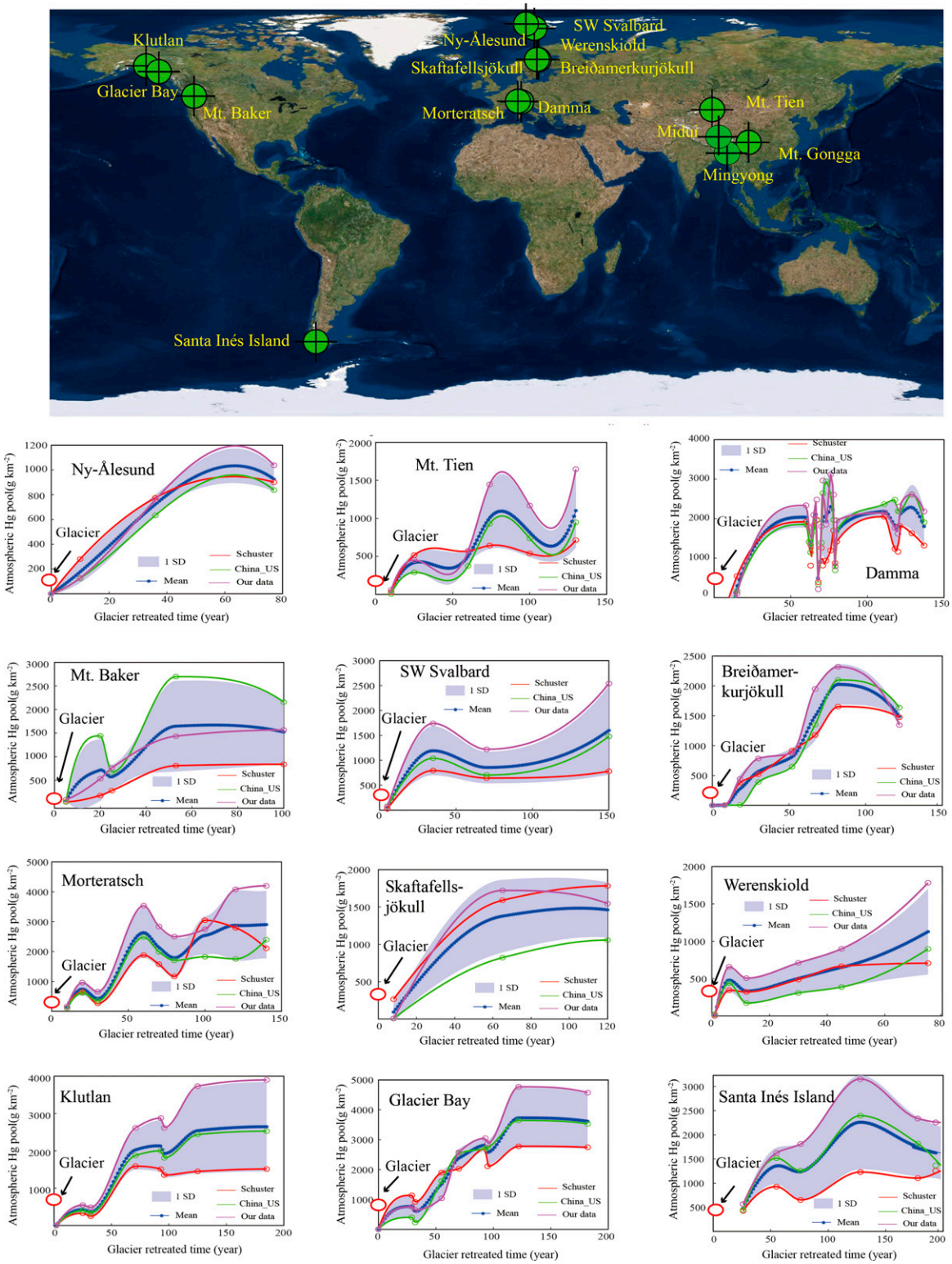

Fig. 3. Hg pool sizes resulted from atmospheric deposition in the surface soil of documented glacier-retreated regions in the world. More detailed information can be found in *SI Appendix*, Table S16. Briefly, the forest succession is for sites of Mt. Gongga (Hailuogou), Midui, Mingyong, Mt. Baker, Morteratsch, southwest (SW) Svalbard, Santa Inés Island, Glacier Bay in Alaska, and Klutlan; the other sites are all in a tundra–shrub/steppe succession.

glacier-retreated areas in the next 100 y [31, 35]) (detailed in *SI Appendix*). Therefore, while glacier melting releases Hg originally locked in the ice into the atmosphere and downstream ecosystems (12, 13, 29), the establishment of new vegetative ecosystems will counter the release through an opposite process that captures atmospheric Hg through glacier-to-vegetation succession. Over a timescale of ~100 y, the latter process is capable of capturing more atmospheric Hg than the Hg released from glacier melt.

Furthermore, glacier melting increases regional water availability (36, 37) and enhances vegetation development well beyond the glacier-retreated regions (38–40). The increased vegetation productivity forced by climate change also occurs in regions where permafrost exists (41, 42). For instance, the warmer and wetter climate in high-altitude alpine regions during 2000 to 2009 has been shown to increase the net primary productivity by 1.28 Pg C in the north hemisphere (41). This represents a net accumulation of ∼60 Mg of Hg over the same period assuming an Hg/C ratio of 50 ng g^{-1} in vegetation (14, 16), which may have contributed to the observed decreasing trend of atmospheric Hg^0 level in these regions over the past 20 y (14). The increased vegetative coverage also cools down soil temperature by 2.7 to 5.7 °C (43), reduces solar irradiation reaching the ground, and therefore, restrains Hg^0 reemission from soil. The net effect of climate warming on Hg cycling in glacier regions needs to be studied further.

Finally, alpine and subpolar glacier coverages have shrunk by 50 to 60% since 1850 (glacier loss area: 7 to 8 × 10^5 km^2) (44–47). Assuming that 10 to 20% of these glacier-retreated regions have since been forested (44–47), 400 to 600 Mg Hg (calculations are in *SI Appendix*) would have been accumulated in the organic soil in these regions since 1850. This may be insignificant compared with the total amount of global primary anthropogenic Hg emissions (∼470 Gg) since 1850 (48). However, our findings on Hg translocation dynamics in glacier-retreated chronosequences show a rare example of an opposite process that counters the previously reported impact of a warming climate on Hg cycling. Glacier-retreated chronosequences provide a natural laboratory to explore the accumulation and availability of Hg in terrestrial ecosystems in a changing climate. Our data show that a mature forest results in greater Hg^0 deposition than a young forest, while a net atmospheric Hg^0 accumulation rate is greater in young forest. This is likely caused by the accelerated increase of biomass growth in a young forest and the different Hg^0 reemission flux from soil. Future studies to understand Hg exchanges in glacier-retreated chronosequence are needed to better assess the fate of atmospheric Hg under a changing climate.

Methods

Sample Collections and Measurements. Detailed information regarding the study sites, sampling, and analytical methods is provided in *SI Appendix*. The Hg isotopic ratios in air, precipitation, soil, and vegetation samples were determined on a Nu-Plasma II multicollector-inductively coupled plasma mass spectrometer.

Mercury MIF Mixing Model. The Hg MIF mixing model and the model uncertainties are described in detail in *SI Appendix*. Briefly, given the unique MIF signatures in atmospheric Hg^0, atmospheric Hg(II), and geological endmembers, the following triple-endmember mixing model is applied to trace Hg sources in soil:

$$F_1 + F_2 + F_3 = 1 \quad [1]$$

$$F_1 \times \Delta^{199}Hg_1 + F_2 \times \Delta^{199}Hg_2 + F_3 \times \Delta^{199}Hg_3 = \Delta^{199}Hgsoil \quad [2]$$

$$F_1 \times \Delta^{200}Hg_1 + F_2 \times \Delta^{200}Hg_2 + F_3 \times \Delta^{200}Hg_3 = \Delta^{200}Hgsoil, \quad [3]$$

where F is the fraction ratio, subscript 1 denotes the atmospheric Hg^0 input, subscript 2 denotes the atmospheric Hg(II) input, and subscript 3 denotes the geological source. The mixing model is constrained using $\delta^{202}Hg$ as follows:

$$0 \le \delta^{202}Hg_{soil} - \left(F_1 \times \delta^{202}Hg_1 + F_2 \times \delta^{202}Hg_2 + F_3 \times \delta^{202}Hg_3\right) \le a, \quad [4]$$

where a is the limit for the shift of $\delta^{202}Hg$ caused by nonsource-mixing processes in soil. The uncertainties caused by the Hg MIF mixing model are described in detail in *SI Appendix*.

SOC–Hg Statistical Model to Estimate Soil Hg Concentration. SOC was used to estimate the soil Hg concentration by 3 regression models (details are in *SI Appendix*). The soil Hg concentrations in documented glacier-retreated regions (Hg_{av}) elsewhere were taken as the average of estimates from 3 different empirical equations. The Hg pool contributed by atmospheric deposition in these regions is estimated using

$$AHgPool = Hg_{av} \times BD \times (1 - f) \times Depth \times (1 - f_{geo}), \quad [5]$$

where BD is the bulk density, f is the volume fraction of coarse material in the surface soil, and f_{geo} is the fraction of geological Hg source estimated by SOC using the data collected at the 3 glacier recession sites (Hailuogou, Mingyong, and Midui). The average atmospheric Hg^0 accumulation rate, original glacier Hg pool size, and Hg mass captured by newly developed vegetation and soil after glacier retreat are described in detail in *SI Appendix*.

Data Availability. Data presented in this study can be found in *SI Appendix*, Tables S1–S19. The GVolume (glacier volume) of each site is from World Glacier Inventory (https://nsidc.org/data-set/G01130/versions/1/form) and Randolph Glacier Inventory 6.0 (https://www.glims.org/RGI/rgi60_dl.html).

ACKNOWLEDGMENTS. This work was funded by the Strategic Priority Research Programs of the Chinese Academy of Sciences; Pan-Third Pole Environment Study for a Green Silk Road Grant XDA2004050201; National Natural Science Foundation of China Grants 41977272, 41829701, 41703135, and 41771062; and the K. C. Wong Education Foundation. The contribution of F.W. was partially supported by the Canada Research Chairs program.

1. H. Zhang *et al.*, Atmospheric mercury inputs in montane soils increase with elevation: Evidence from mercury isotope signatures. *Sci. Rep.* **3**, 3322 (2013).
2. R. S. Yin *et al.*, Historical records of mercury stable isotopes in sediments of Tibetan lakes. *Sci. Rep.* **6**, 23332 (2016).
3. D. Obrist *et al.*, Tundra uptake of atmospheric elemental mercury drives Arctic mercury pollution. *Nature* **547**, 201–204 (2017).
4. X. Wang *et al.*, Using mercury isotopes to understand mercury accumulation in the montane forest floor of the Eastern Tibetan Plateau. *Environ. Sci. Technol.* **51**, 801–809 (2017).
5. D. Obrist *et al.*, A review of global environmental mercury processes in response to human and natural perturbations: Changes of emissions, climate, and land use. *Ambio* **47**, 116–140 (2018).
6. M. Dyurgerov, Mountain and subpolar glaciers show an increase in sensitivity to climate warming and intensification of the water cycle. *J. Hydrol.* **282**, 164–176 (2003).
7. M. B. Dyurgerov, M. F. Meier, Mass balance of mountain and subpolar glaciers: A new global assessment for 1961-1990. *Arct. Alp. Res.* **29**, 379–391 (1997).
8. F. Brun, E. Berthier, P. Wagnon, A. Kaab, D. Treichler, A spatially resolved estimate of High Mountain Asia glacier mass balances from 2000 to 2016. *Nat. Geosci.* **10**, 668–673(2017).
9. T. D. Yao *et al.*, Different glacier status with atmospheric circulations in Tibetan Plateau and surroundings. *Nat. Clim. Chang.* **2**, 663–667 (2012).
10. X. Sun *et al.*, The role of melting alpine glaciers in mercury export and transport: An intensive sampling campaign in the Qugaqie Basin, inland Tibetan Plateau. *Environ. Pollut.* **220**, 936–945 (2017).
11. J. Huang *et al.*, Mercury distribution and variation on a high-elevation mountain glacier on the northern boundary of the Tibetan Plateau. *Atmos. Environ.* **96**, 27–36 (2014).
12. Q. Zhang *et al.*, Mercury distribution and deposition in glacier snow over western China. *Environ. Sci. Technol.* **46**, 5404–5413 (2012).
13. J. Søndergaard *et al.*, Mercury exports from a high-Arctic river basin in Northeast Greenland (74°N) largely controlled by glacial lake outburst floods. *Sci. Total Environ.* **514**, 83–91 (2015).
14. M. Jiskra *et al.*, A vegetation control on seasonal variations in global atmospheric mercury concentrations. *Nat. Geosci.* **11**, 244–250 (2018).
15. W. Zheng, D. Obrist, D. Weis, B. A. Bergquist, Mercury isotope compositions across North American forests. *Global Biogeochem. Cycles* **30**, 1475–1492 (2016).
16. X. Wang *et al.*, Enhanced accumulation and storage of mercury on subtropical evergreen forest floor: Implications on mercury budget in global forest ecosystems. *J. Geophys. Res. Biogeosci.* **121**, 2096–2109 (2016).
17. X. Wang *et al.*, Effects of precipitation on mercury accumulation on subtropical montane forest floor: Implications on climate forcing. *J. Geophys. Res. Biogeosci.* **124**, 959–972 (2019).
18. J. D. Blum, L. S. Sherman, M. W. Johnson, Mercury isotopes in earth and environmental sciences. *Annu. Rev. Earth Planet. Sci.* **42**, 249–269 (2014).
19. J. E. Sonke, A global model of mass independent mercury stable isotope fractionation. *Geochim. Cosmochim. Acta* **75**, 4577–4590 (2011).
20. M. Enrico *et al.*, Atmospheric mercury transfer to peat bogs dominated by gaseous elemental mercury dry deposition. *Environ. Sci. Technol.* **50**, 2405–2412 (2016).
21. M. Jiskra *et al.*, Mercury deposition and re-emission pathways in boreal forest soils investigated with Hg isotope signatures. *Environ. Sci. Technol.* **49**, 7188–7196 (2015).
22. J. D. Demers, J. D. Blum, D. R. Zak, Mercury isotopes in a forested ecosystem: Implications for air-surface exchange dynamics and the global mercury cycle. *Global Biogeochem. Cycles* **27**, 222–238 (2013).
23. J. B. Richardson, A. J. Friedland, Mercury in coniferous and deciduous upland forests in northern New England, USA: Implications of climate change. *Biogeosciences* **12**, 6737–6749 (2015).

24. D. Obrist, D. W. Johnson, R. L. Edmonds, Effects of vegetation type on mercury concentrations and pools in two adjacent coniferous and deciduous forests. *J. Plant Nutr. Soil Sci.* **175**, 68–77 (2012).
25. T. Navrátil *et al*., Distribution and pools of mercury in Czech forest soils. *Water Air Soil Pollut.* **225**, 1829 (2014).
26. J. I. Juillerat, D. S. Ross, M. S. Bank, Mercury in litterfall and upper soil horizons in forested ecosystems in Vermont, USA. *Environ. Toxicol. Chem.* **31**, 1720–1729 (2012).
27. H. M. Amos *et al*., Observational and modeling constraints on global anthropogenic enrichment of mercury. *Environ. Sci. Technol.* **49**, 4036–4047 (2015).
28. X. Wang, Z. Bao, C.-J. Lin, W. Yuan, X. Feng, Assessment of global mercury deposition through litterfall. *Environ. Sci. Technol.* **50**, 8548–8557 (2016).
29. P. F. Schuster *et al*., Permafrost stores a globally significant amount of mercury. *Geophys. Res. Lett.* **45**, 1463–1471 (2018).
30. A. E. Raftery, A. Zimmer, D. M. W. Frierson, R. Startz, P. R. Liu, Less than 2 degrees C warming by 2100 unlikely. *Nat. Clim. Change* **7**, 637–641 (2017).
31. V. Radic, R. Hock, Regionally differentiated contribution of mountain glaciers and ice caps to future sea-level rise. *Nat. Geosci.* **4**, 91–94 (2011).
32. M. Zemp, W. Haeberli, M. Hoelzle, F. Paul, Alpine glaciers to disappear within decades? *Geophys. Res. Lett.* **33**, L13504 (2006).
33. J. L. Chen, C. R. Wilson, B. D. Tapley, Contribution of ice sheet and mountain glacier melt to recent sea level rise. *Nat. Geosci.* **6**, 549–552 (2013).
34. G. K. C. Clarke, A. H. Jarosch, F. S. Anslow, V. Radic, B. Menounos, Projected deglaciation of western Canada in the twenty-first century. *Nat. Geosci.* **8**, 372–377 (2015).
35. J.-B. Bosson, M. Huss, E. Osipova, Disappearing world heritage glaciers as a keystone of nature conservation in a changing climate. *Earths Futur.* **7**, 469–479 (2019).
36. S. Liu *et al*., Glacier retreat as a result of climate warming and increased precipitation in the Tarim river basin, northwest China. *Ann. Glaciol.* **43**, 91–96 (2006).
37. J. Crossman, M. N. Futter, P. G. Whitehead, The significance of shifts in precipitation patterns: Modelling the impacts of climate change and glacier retreat on extreme flood events in Denali National Park, Alaska. *PLoS One* **8**, e74054 (2013).
38. R. Zhang *et al*., Impact of climate change on vegetation growth in Arid Northwest of China from 1982 to 2011. *Remote Sens.* **8**, 364 (2016).
39. G. J. Jia, H. E. Epstein, D. A. Walker, Vegetation greening in the Canadian Arctic related to decadal warming. *J. Environ. Monit.* **11**, 2231–2238 (2009).
40. F. L. Marchand *et al*., Climate warming postpones senescence in high Arctic tundra. *Arct. Antarct. Alp. Res.* **36**, 390–394 (2004).
41. M. Zhao, S. W. Running, Drought-induced reduction in global terrestrial net primary production from 2000 through 2009. *Science* **329**, 940–943 (2010).
42. J. Z. Ding *et al*., Decadal soil carbon accumulation across Tibetan permafrost regions. *Nat. Geosci.* **10**, 420–424 (2017).
43. P. Porada, A. Ekici, C. Beer, Effects of bryophyte and lichen cover on permafrost soil temperature at large scale. *Cryosphere* **10**, 2291–2315 (2016).
44. E. Y. Osipov, O. P. Osipova, Mountain glaciers of southeast Siberia: Current state and changes since the Little Ice Age. *Ann. Glaciol.* **55**, 167–176 (2014).
45. M. Zemp, F. Paul, M. Hoelzle, W. Haeberli, "Glacier fluctuations in the European Alps, 1850–2000" in Darkening Peaks*: Glacier* Retreat, Science, and Society, B. Orlove, E. Wiegandt, B. H. Luckman, Eds. (University of California Press, 2008), pp. 152–167.
46. J. A. Smith *et al*., Sub-ice-shelf sediments record history of twentieth-century retreat of Pine Island glacier. *Nature* **541**, 77–80 (2017).
47. G. H. Roe, M. B. Baker, F. Herla, Centennial glacier retreat as categorical evidence of regional climate change. *Nat. Geosci.* **10**, 95–99 (2017).
48. D. G. Streets *et al*., Total mercury released to the environment by human activities. *Environ. Sci. Technol.* **51**, 5969–5977 (2017).